ELUCIDATING SURFACE SITES AND REACTIVITY OF A ZIRCONIUM-BASED MOF TOWARDS FUTURE CAPPING AND TRAPPING OF GUEST MOLECULES

WPI

Rebecca A. Dawley

A Major Qualifying Project Report
in partial fulfillment of the requirements for the
Degree of Bachelor of Science in Chemistry
submitted to the Faculty of

WORCESTER POLYTECHNIC INSTITUTE
100 Institute Road
Worcester, Massachusetts 01609

Typeset in LaTeX. Printed in the United States of America.

CONTENTS

LIST OF FIGURES

PREFACE

UiO–66, a zirconium-based metal organic framework (MOF), was synthesized to investigate surface-level interactions. We are interested in expanding our understanding of MOFs and their ability to cap, trap, and store guest molecules within their porous 3-D structures, applicable for drug delivery. We hypothesize that fluorocarbon silanes will interact with UiO–66 terminal oxygen species to form strong covalent bonds. Synthesized by previously established solvothermal methods, UiO–66 crystals were incorporated in a series of experiments to investigate interfacial states and attachment strategies for capping and trapping. *In vacuo* heating and Ar^+ sputtering experiments further supported the binding interaction between the silane and the UiO–66 itself. Analytical techniques including thermogravimetric analysis (TGA), X-ray photoelectron spectroscopy (XPS), and powder X-ray diffraction (pXRD) were used to evaluate the effectiveness of developed methods. We have demonstrated that silanes attached to a UiO–66 surface provides a method for establishing monolayer chemistry that is compatible with this specific MOF family.

GLOSSARY

BDC	benzene dicarboxylic acid *a.k.a.* terephthalic acid
DCM	dichloromethane
DEF	diethylformamide
fwhm	full-width-at-half-maximum
IPA	*iso*propyl alcohol
MOF	metal-organic framework
PTFE	*poly*-(tetrafluoroethylene)
TGA	thermogravimetric analysis
UHV	ultrahigh vacuum
XPS	X-ray photoelectron spectra/spectroscopy
XRD	X-ray diffraction

CHAPTER 1

INTRODUCTION

Metal organic frameworks (MOFs) are multidimensional organic-inorganic hybrid materials known for their porous nature, high internal surface areas, and tunable chemistries.[1–2] Generally, they consist of metal centers coordinated by bridging organic ligands, also known as linkers, to form a robust crystalline network.[1–3] As a result of this connectivity, permanent porosity is established amongst metal centers, allowing for other species to enter and exit the frameworks through adsorption.[1,4–5] By varying the length of organic linker chains, both the pore sizes and internal surface areas of MOFs can be modified, usually without impacting its chemistry.[3,6] The vast flexibility resulting from linker and inorganic cluster combinations has yielded over 20,000 distinct MOF structures to date.[1] The unique yet adjustable nature of MOFs enables them to act as matrices for applications including catalysis,[3] gas storage,[7] as well as selective gas and solvent separations.[8]

Among the myriad applications, we are particularly intrigued by the potential use of these materials as drug delivery vehicles.[3,6,9–10] Adequate biocompatibility, controlled release in vivo of drugs with high loading rates, and ability to be catabolized are essential for success in bio-therapeutic applications.[11]

The customizable properties including stability and size found in MOFs make them viable targets for further development as nanocarriers.[10–11] MOFs provide a contained space for guest molecules, that we envision to be therapeutic small-molecule drugs.[6] MOFs have shown great potential as vectors in drug delivery, hence motivating further studies to control the rate and on command release of stored guests.

One strategy for implementing controlled release utilizes modifications of the MOF's surface to further trap molecular guests.[4–5,10,12–13] Post-synthetic methods allow the MOF surface of interest to be modified through techniques including the introduction of a capping species via click modulation[14] and coating with polymers.[15] There is research out there exploring other methods of MOF modification including post synthetic ligand exchange,[2,16–17] minimizing linker defects,[18–19] and the functionalization of internal pore surface.[9] However, as we are focused on surface derivatization, the specifics will not be discussed further in this study. Few reports undertake the covalent surface attachment of capping molecules, hence motivating the work of our group.[4–5,12–13]

Among capping strategies, direct covalent attachment of capping molecules is particularly compelling. The motivation for establishing a strong covalent attachment lies in overall stability of a covalent bond between the capping group and the MOF, as well as increased flexibility for exogenous activation that may occur at some other chemical group along capping molecule.[5] The desire for strong, covalent attachment of capping groups to a MOF surface drives the need to understand chemical species on the surface of that MOF, and how those can be exploited for cap attachment and possibly for effective guest release. The insight gained from establishing surface species and cap bonding interactions should enable explorations of the role of stimuli for exogenous or endogenous activation that would trigger guest release. For instance, work in other labs has demonstrated the activation and release of guests from MOF structures by light, heat, or pH.[10] Our lab demonstrated the release of guests from MOF–5 based on the UV photodegradation of a nitrophenyl-containing capping molecule.[5] Despite MOF–5's ease of synthesis and large pores, may not be viable for therapeutic drug delivery based on its instability in humid air and under acidic conditions. The lack of long-term stability in MOF–5 drives our interest in exploring the surface chemistry and capping of more robust, alternative frameworks.

Zirconium terephthalate MOF UiO–66, Fig. 1.1, may be an effective alternative to MOF–5 due to its reported stability in various conditions including air, water, and other solvents.[1,8,16–18,20] Of course, resistance to water is potentially necessary for drug delivery applications where biocompatibility is a driving factor for effectiveness.[12] Despite the extensive research of UiO–66 crystals, knowledge gaps remain regarding the terminal species existing on the MOF and establishing covalent derivatization of those species.

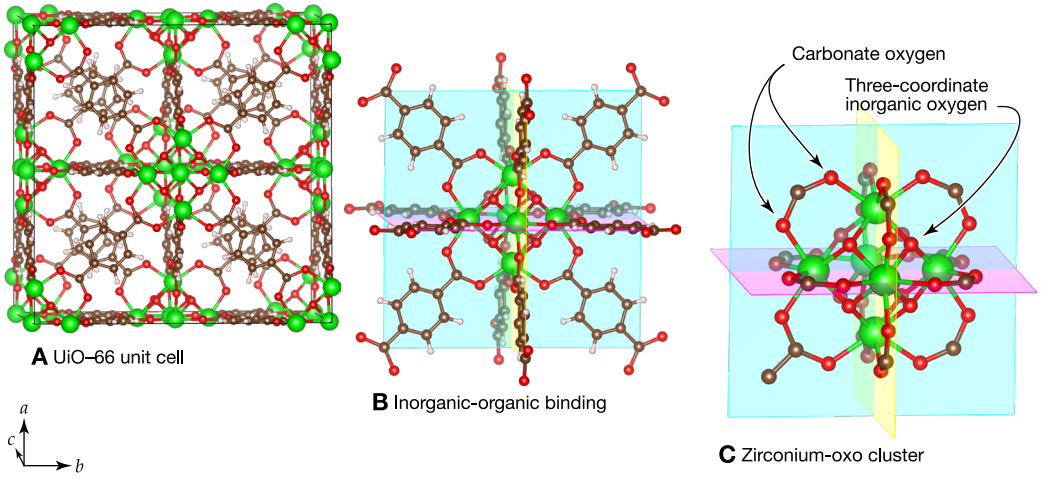

Figure 1.1 Crystal structure of UiO–66 at: A one full UiO–66 unit cell, B one cluster bound to terephthalate ligand, and C zirconium oxo cluster with further magnification.

Figure 1.1 reveals the interconnectedness of zirconium-oxygen clusters with 1,4-benzenedicarboxylate (BDC) linkers and informs our hypothesis for bonding with capping molecules.[2,8,18] From one unit cell in Fig. 1.1A, a focusing on an individual inorganic cluster in Fig. 1.1B reveals a network of $Zr_6O_4(OH)_4$ clusters that are each connected to twelve BDC linkers. Further magnification in Fig. 1.1C highlights two types of bonding configuration at oxygen atoms. One oxygen configuration consists of three-coordinate bonding between an oxygen atom and adjacent zirconium atoms, while other oxygen atoms from the carbonate moieties on deprotonated BDC principally interact with only one zirconium atom. Notably, Fig. 1.1 shows inorganic clusters as Zr_6O_8 structures rather than $Zr_6O_4(OH)_4$ from published crystal structures.[2] The hydroxyl hydrogen atoms are not included as they likely occupy four different locations around the eight inorganic oxygen atoms in each cluster. Such random distribution of hydrogen atoms likely appears as scattering from "half" of a hydrogen atom's electron density in the diffraction data of a real UiO–66 crystal. Further support for the presence of hydroxyl species comes from the overall balance of charge at each inorganic cluster. The bonding of twelve BDC molecules via carbonate groups with a –1 charge implies a charge of +12 on each inorganic cluster. For a +12 charge, six Zr^{4+} are well balanced by four O^{2-} and four $(OH)^-$ species. The model of bonding at the inorganic clusters informs our hypothesis about what chemical states might exist on a UiO–66 crystal surface, and how we might form interactions with a capping group. Among these crystal structures there are Zr–OH and Zr–O–Zr moieties. Of particular interest, Zr–OH moieties demonstrate amphoteric or purely basic behavior,[21] and thus should be reactive towards acidic silanes that form monolayers on metal oxide surfaces at hydroxyl sites.[22] Thus we hypothesize that silanes should form monolayers on UiO–66 surfaces that could lead to future capping and trapping of guests within the UiO family of structures. Testing this hypothesis of silane capping motivates our present investigations.

Herein, we synthesized single-crystal UiO–66 to interact with a silane solution and test our hypothesis that oxygen on zirconium complexes will readily form bonds with silane silicon to establish an interfacial covalent bond between UiO–66 and silane monolayers. Thermogravimetric analysis (TGA) and powder X-ray diffraction (pXRD) supported the synthesis of crystalline UiO–66 material. X-ray photoelectron spectroscopy (XPS) established the atomic surface speciation both for nascent and for silane-exposed UiO–66 material. We utilized in vacuo heating and argon-ion sputtering to further support the binding interaction between the silane and the UiO–66 itself. The results enable new modalities for surface attachment to the UiO family of MOFs towards the future capping and trapping of guest molecules within therapeutic drug delivery applications.

CHAPTER 2

EXPERIMENTAL SECTION

2.1 Materials and Chemicals

All chemicals were used as received unless otherwise noted. Chemicals used in the synthesis and capping of metal organic framework UiO–66 included zirconium dichloride oxide hydrate ($ZrOCl_2 \cdot xH_2O$, 99.9% metals basis, Alfa Aesar), terephthalic acid (BDC, 99+%, Acros Organics), and trichloro(1H,1H,2H,2H-perfluorooctyl) silane (97%, Sigma Aldrich). N,N-diethylformamide (DEF, >99%, Tokyo Chemical Industry) was run through a silica column prior to use and any leftover solvent following synthesis was stored in a desiccator for later use. Formic acid (98+%pure, Acros Organics), dichloromethane(99.5%,VWR Chemicals BDH),dry toluene (>99.5%, Fisher Scientific) obtained from a Grubbs-type solvent purification system, and isopropanol (IPA, 99.6%, Acros Organics) were also used during experimentation.

2.2 Instrumentation

The instrument used for thermogravimetric analysis was a TA Instruments Hi-Res TGA 2950 Thermogravimetric Analyzer.[5]

An argon-purged (ultrahigh purity, UHP, Airgas) Schlenk line equipped with an oil diffusion pump having a base pressure less than 1×10^{-3} torr was used for vacuum degassing of MOF samples.

Powder X-ray Diffraction data was collected on a Bruker-AXS D8-Advance diffractometer using Cu-Kα radiation with X-rays generated at 40 kV and 40 mA.

During synthesis, samples were cooked in a Yamato constant temperature drying oven, model DVS402, set at 173 °C, meaning the in oven temperature was 135 °C as measured at a K-type thermocouple that was positioned directly adjacent to the sample reaction glassware.

A PHI 5600 XPS system with a third-party data acquisition system (RBD Instruments, Bend Oregon) acquired all X-ray photoelectron (XP) spectra as discussed in prior publications.[23–27] Analysis chamber base pressures were around 1×10^{-9} torr. A hemispherical energy analyzer collected the X-ray photoelectrons. A monochromated Al Kα source produced X-rays at a 90° angle with respect the takeoff angle for the energy analyzer. For this experiment, XPS data collection utilized a level sample puck that yields 45° angles both for the incoming monochromated X-radiation and for the photoelectron take-off angle with respect to the sample normal angle. In all experiments, survey spectra utilized a 117 eV pass energy, a 0.5 eV step size, and a 50-ms-per-step dwell time. All high-resolution XP spectra employed a 23.5 eV pass energy, 0.025 eV step size, and a 50 ms dwell time per step.

X-ray photoelectron acquisitions included wide-energy survey scans as well as high-resolution scans of the C 1s, O 1s, Si 2p, Zr 3d, and F 1s regions for all samples. All samples required charge neutralization. Neutralization parameters were optimized to yield a C 1s feature from adventitious contaminants of minimal full-width-at-half maximum (fwhm) value that was corrected to 285.0 eV during analysis following scanning.

Peak quantification utilized an in-house-developed LabVIEW program based on published spectral shapes and corrected for instrument-specific sensitivity factors,[28–29] and background-energy-loss functions.[30–32] Data fitting employed baseline-corrected, pseudo-Voigt, GL(x)-style functions where x nonlinearly scales from a pure Gaussian ($x = 0$) to a pure Lorentzian ($x = 100$). Fits with multiple peaks (Si 2p, Zr 3d) within a spectral region were constrained to identical full-width-at-half-maximum (fwmh) values for each peak within the region.

2.3 Synthesis of Single Crystal UiO–66

We based our MOF synthesis on previously reported procedures from Boissonnault and co-workers,[16] as well as Trickett and co-workers.[19] Minor adjustments were made to yield the best crystals using the materials and equipment available to us. Samples were usually prepared in groups of two to three for efficiency purposes. The oven used for synthesis was preheated to set point 173 °C prior to gathering synthesis materials. Separate experiments revealed a disparity between the set point temperature and in oven temperature as measured at a K-type thermocouple sitting millimeters from the sample. Differences between the set value and in oven temperature were consistently 30–40 degrees off in a typical experiment. In this case, the set point value is 173 °C and in oven temperature is 135 °C. Vials and their caps, along with a spatula, were pumped into the lab space's shared recirculating glovebox using three 5–10 min cycles. 12 mg of $ZrOCl_2$ was measured into each vial and brought out of the glovebox. The remainder of the process was performed relatively quickly to minimize air and moisture exposure. The metal salt was dissolved in 2 mL of DEF using sonication. In a separate container, a stock solution composed of 5.2 mg BDC for each milliliter of DEF was prepared and dissolved using sonication. This stock solution was used for multiple MOF syntheses and was never prepared in quantities above 20 mL to ensure it would be used up in a week's time. A milliliter of stock solution was added with a micropipette to the vial containing the dissolved zirconium salt. An extra milliliter of DEF was added to each vial followed by the addition of 4 mL formic acid (1:1 ratio DEF: formic acid) to act as a modulator. The vials were capped, placed in a large beaker in the oven and cooked at 135 °C for 48 h. Following synthesis, all MOF material was stored in the DEF/formic acid solution until time of characterization or capping.

We utilized procedures for the above synthesis that explored the impact of varying reaction vessels, temperatures, and reagent purities. In our case, using capped vials with minor adjustments to published protocols worked the best. More information regarding these experiments can be found in the supplemental information.

2.4 Sample Preparation for Characterization of UiO–66 Single Crystals

Sample vials were opened using slip-joint pliers. The DEF/formic acid mother liqueur was carefully decanted, ensuring as much crystalline material as possible remained inside of — and at the bottom of — the reaction vessel. After decanting, excess DCM (~10–15 mL) was added to the reaction vessel and left to settle for about 15 min before proceeding. DCM was then decanted off and replaced with more DCM. This solvent exchange process was repeated two more times to ensure that DEF was mostly out of solution and on the final time the UiO crystals were suspended in minimal volumes of DCM.

New caps were loosely placed on the vials. After the DCM fully evaporated, the resulting dry crystalline material was used for characterization.

2.5 Characterization of UiO–66 Single Crystals

Thermogravimetric analysis (TGA) measurements were performed using a TA Instruments Hi-Res TGA 2950 Thermogravimetric Analyzer[5] from room temperature to 600 °C under ambient atmosphere at a heating rate of 10 °C min^{-1}. The experimental spectrum was compared to those displayed previously in published literature to confirm identity of synthesized samples.[18–19]

Powder X-ray Diffraction data was collected on a Bruker-AXS D8-Advance diffractometer using Cu-Kα radiation with X-rays generated at 40 kV and 40 mA. Crystals were mounted using carbon tape on a Teflon sample holder and tape was added to either side. A visual representation of the mounted crystals can be found in the SI. The sample was scanned at RT from 5° to 35° (2θ) in 0.01° steps with a twenty second integration period. Simulated pXRD patterns from the crystal's CIF file were compared to our experimental UiO–66 scan to further support the successful synthesis and identity of our crystalline sample.

2.6 Post Synthetic Silane Capping Procedure

To begin, 15 mL of a 500 μM solution of trichloro(1H,1H,2H,2H-perfluorooctyl) silane was prepared in dry toluene obtained from a Grubbs-type solvent purification system. This solution was stored in the refrigerator until its use the same day.

Sample vials were opened using slip-joint pliers. The DEF/formic acid mother liqueur was carefully decanted, ensuring as much crystalline material as possible remained inside of and at the bottom of the reaction vessel. After decanting, excess DCM (~10–15 mL) was added to the reaction vessel and left to settle for about 15 minutes before proceeding. This solvent exchange process was repeated two more times to ensure that DEF was mostly out of solution. At this point, all DCM was decanted off. The crystalline material was exposed to excess fluorinated silane for five minutes. Directly following the five-minute exposure to the capping molecule, the silane solution was decanted off and crystals were subsequently washed with DCM. The capped UiO–66 MOF was immediately transferred to an XPS puck with epoxy using a spatula to prepare for analysis.

2.7 XPS sample preparation

The most recent version of this utilized centrifugation at 3900 rpm for 2 min, yielding concentrated crystals. A pipet was used for removal of nearly all solvent. UiO–66 crystals were then resuspended by agitation with spatula in a minimal quantity of solvent. The suspended crystals were directly applied onto a XPS puck which was polished with 1200-grit sandpaper and successively rinsed with soap water, water, then isopropanol. The puck with the suspended sample was inserted into vacuum oven held at 100 °C and evacuated with a house rough pump vacuum. Sample remained in oven for ~2 days prior to pumping into XPS instrument for three hours. The process for preparing nascent and capped samples is the same besides the further steps required for capping described in the previous section.

Prior versions consisted of mounting crystals onto the puck using either LOCTITE 1C epoxy adhesive that was set for 60 minutes at 100 °C prior to vacuum heating or carbon tape. Crystals were prepared using the methodology discussed in section 2.4 and if they were also capped the methodology in §2.6 was followed as well. The puck was then placed under vacuum in a drying chamber on the Schlenk line for ~2 days while simultaneously heating at 140 °C. The puck was then left in the XPS load lock overnight to ensure MOF samples were fully degassed prior to scanning.

2.8 Heating and Sputtering of Fluorinated Silane-Derivatized UiO–66

Following the initial XP scan, the stage was heated at 200 °C for 15 minutes and left to cool for roughly 30 minutes. Another scan was initiated using the same automation multiplex settings, adjusting the instrument's neutralizer as necessary, to allow for adequate comparison.

After the completion of the post heating scan, the derivatized, heated sample was bombarded with a flow of argon-ions for 12 seconds to sputter surface monolayers of UiO–66 MOF material. Conditions utilized a differentially pumped ion gun source at 25 mA electron emission, 3.5 kV beam voltage, and $\sim 1.5 \times 10^{-4}$ Torr of research-grade argon.[4] Sputtering occurred in an expanded area of the MOF aligned with the sampling region of the XPS instrument. Previous experiments revealed our instrument effectively removes roughly one monolayer off the surface per every six seconds of exposure to argon-ions. Similar to the heating experiment, XP multiplex scans were initiated immediately following described methods to observe chemical species present post sputtering.

CHAPTER 3

RESULTS

3.1 TGA Characterization

When compared to previously published TGAs,[18–19] our experimental spectrum was nearly identical and can be found in the supporting information. Three major steps are observed, indicating the loss of water, organic species, and finally the decomposition of the terephthalate linker.[19] The onset of steps occurred around the same temperatures in comparison to those in the literature. There are slight shifts in the temperatures as well as the mass loss percentages, likely due to the quantity and dryness of the crystals being observed. Overall, the curvature of the data is generally the same, supporting the successful synthesis of single crystal UiO–66.

3.2 Powder X-ray Diffraction (pXRD) Characterization

The experimentally determined PXRD pattern was compared to simulated patterns for UiO–66 using VESTA software. Our scan was also compared to published single crystal UiO–66 PXRD data.[19] The scan was performed at very

high resolution for a small range of 2θ in order to get stronger signal for the known prominent peaks in smaller angles of this scan and can be found in the supplemental information. The reflections located at 2θ values 7.38°, 8.59°, and 12.069° confirm the identity of the synthesized UiO–66 MOF because they align with established values collected by Øien and collaborators.[18] Of important note in our pXRD results is the large peak at about 18° 2θ, representing the PTFE (Teflon) sample holder and not sample contamination.[33] A program developed in house was used to evaluate the average crystal size incorporating the Scherrer equation, yielding single crystals of about 20 nm in size.

3.3 X-ray Photoelectron Spectroscopy (XPS)

The motivation for using a fluorinated silane in this study results from its distinguished and enhanced signal while using XP instrumentation. By monitoring the presence or absence of this fluorine chemical species, we can observe whether the capping molecule of interest is present on the MOF crystals being analyzed. From there, understanding its localization and potential attachment can be probed using heating and argon-ion sputtering methods. Figure 3.1 depicts the characteristic X-ray photoelectron regions of Zr 3d, Si 2p, C 1s, F 1s, O 1s, Cl 2p relating to our proposed MOF surface attachment strategies. Fig. 3.1A depicts nascent UiO–66 crystals, previously analyzed with thermogravimetric and powder X-ray diffraction. As expected, there is no F 1s signal present since the nascent species acts as a control for evaluating the establishment of a strong covalent bond between the MOF surface and surface capping molecules. For all frames, we ascribe blue-shaded features in the Zr 3d and O 1s regions to the signals resulting from their connectivity to one another within the framework. In the nascent sample, the relative intensities of the Zr 3d doublet and the metal oxide signal appearing at ~531 eV of the O 1s region are more prominent considering only the UiO–66 is being scanned. Fig. 3.1B displays the representative photoelectron regions of UiO–66 following 5 minutes of exposure to 500 μM of trichloro(1H,1H,2H,2H-perfluorooctyl) silane. The green colored fitted features in frames B–D depicts the F 1s XP region as well as the contributions in the C 1s region at ~292 eV corresponding to bonds with fluorine.[29] We see no feature ascribable to Cl 2p (usually found at 198.5 eV)[29] above the broad zirconium inelastic scatter in the range 194–204 eV. The presence of fluorine and absence of chlorine, considering its original presence in the capping molecule, implies a covalent transformation of this species. Upon introduction of the silane, there are more carbon and fluorine chemical species present on the MOF surface being analyzed, and as a result a decrease in both zirconium and oxygen's presence. This can be observed through the appearance of green features and reduction of blue feature areas. The knowledge gaps that remain after establishing the silane's presence on UiO–66 samples is if the molecule is covalently bound

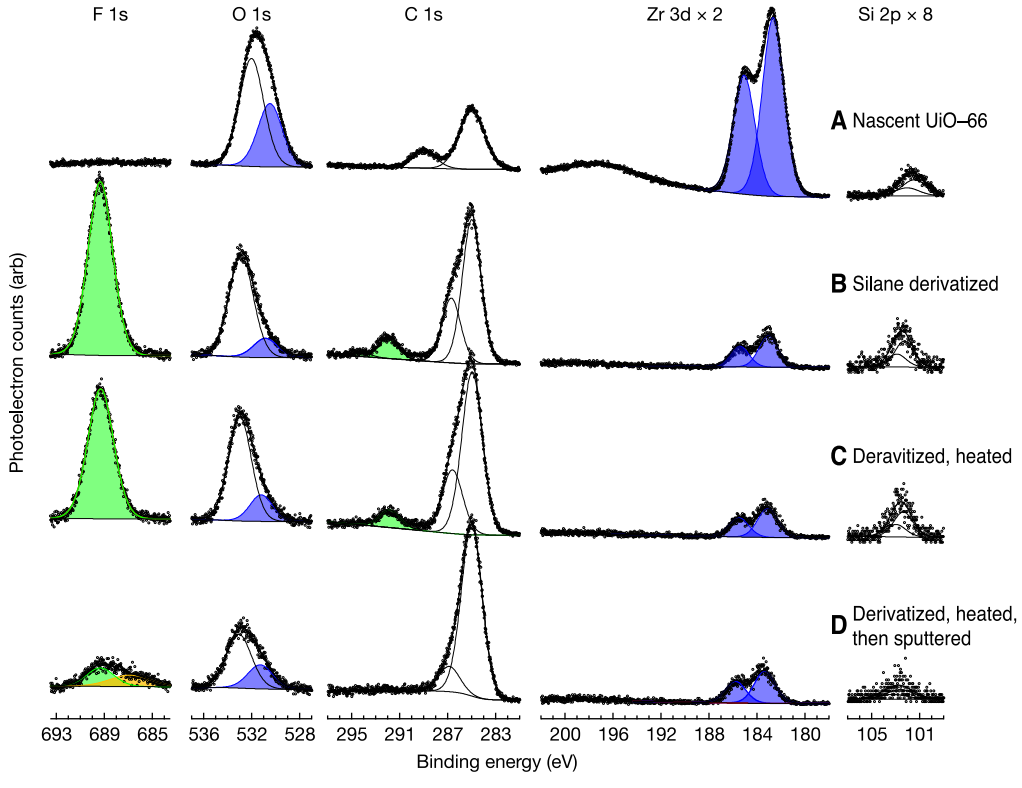

Figure 3.1 Representative XP spectra of (**A**) nascent single-crystal UiO–66, (**B**) Derivatized with the fluorinated silane, (**C**) Derivatized UiO–66 after 15 min at 200 °C heating, and (**D**) Derivatized, heated, then Ar^+ sputtered for 12 s to remove ~2 surface monlayers.

and if so, its localization, whether it be within the MOF or on the surface. Fig. 3.1C displays the impact of silane derivatization followed by 15 min of heating at 200 °C on UiO–66 single crystals. In theory, heating within the XPS chamber should remove any species that are not strongly bound to something else. In comparison to the previous frame showing the silane derivatized MOF prior to heating methods, they appear nearly identical. The continued appearance of fluorine at ~689 eV further supports our hypothesis that silanes will readily form a strong covalent bond with UiO–66. Now remains the uncertainty of where the silane is bound, which can be explored further using argon-ion sputtering methodologies. Fig. 3.1D demonstrates UiO–66 samples following derivatization, heating, and finally 12 s of Ar^+ sputtering. In separate experiments performed by Alex Carl and Julia Martin our group established that a 6 s sputter under identical conditions removes one monolayer of iridium oxide on iridium.[4] Thus a 12 s exposure should ~1–2 monolayers from the MOF's surface, hence enabling observations to be made regarding interfacial covalent bonding. The fluorine feature is nearly diminished following this procedure as can be seen with the green fitted peak. A new chemical species, an orange fitted feature within the figure, emerges at ~687 eV. In the process of sputtering and desorbing interfacial bonds, a restructuring likely occurs as seen by the lower binding energy indicating fluorides. Regardless, this featured does not sit in the same location of ~689 eV where carbon fluorine bonds have been noticeable in frames B and C. Also, there is no longer a distinguishable feature in the C 1s region attributed to connectivity with fluorine. It is important to note that some amount of the fluorine attributed to the capping species remains. This is likely a result of some challenges attributed to sputtering, including varied sample geometry and orientation.[17] Of particular note, there is a silicon feature displayed in the nascent XP scan despite there being no capping molecule present or silicon within the framework. The Si 2p appearance in nascent UiO–66 is shifted lower, located at ~102 eV in comparison to the feature from the silane molecule occurring at ~103 eV. This indicates the nascent sample has a distinct silicon contamination, likely from factors potentially including residual pump oil vapor from the vacuum, residual silicon in the XPS chamber, or even glassware during synthesis.[34]

CHAPTER 4

DISCUSSION

4.1 Synthesis and Characterization of Single Crystal UiO–66

By comparing experimental pXRD and TGA results with previous publications, we concluded our slightly modified synthesis of UiO–66 single crystal MOF was successful. Despite its confirmed identity, there was some run to run variability of the syntheses for this MOF overall. The seal of the reaction vessel was not reliable, therefore making it difficult to predict how much solvent would evaporate during the cooking period and keep the final volume of both DEF and formic acid constant for all samples. Prior research has explored how varying the ratio of DEF:formic acid modulator has a noticeable impact on resulting crystal size.[19] Additional variability could have been introduced with temperature fluctuations in the oven, as that has posed some challenges in the past. Generally, control over crystallization kinetics can be difficult with the highly specific reaction conditions for many MOFs, including this one.[35] Also, it is unclear whether or not the solvent exchange with DCM is necessary prior to characterization and if that impacts the crystals. Prior group research concluded that solvent exchange using MOF–5 crystals rounded crystal corners, and perhaps that is the same with UiO–66 material.

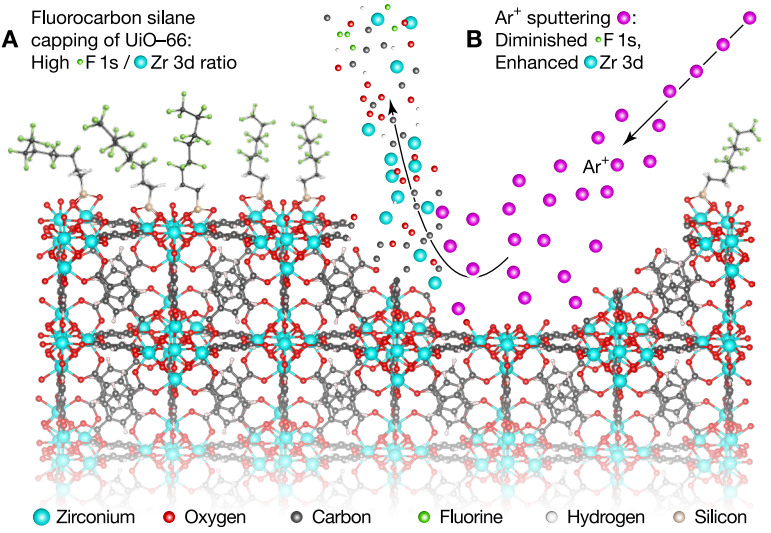

Figure 4.1 A model consistent with our experimental data for silane attachment to UiO–66 surfaces. Frame (**A**) depicts this bond occurring at inorganic oxygens and what we predict from the corresponding XPS data for this surface attachment. Frame (**B**) shows the impact of Ar^+ sputtering as surface monolayers are removed, hence impacting the specific features and intensities we see in XPS scans following ion sputtering.

4.2 X-ray Photoelectron Spectroscopy

Our data supports the hypothesis of an interfacial, covalent bond between single crystal UiO–66 and trichloro(1H,1H,2H,2H-perfluorooctyl) silane. Figure 4.1 displays a model representing the data as well as our original hypothesis. Upon UiO–66's exposure to the fluorocarbon silane, representative chemical species, especially fluorine, confirmed the capping molecule's presence among the single crystals. However, the simple appearance of a fluorine signal following its exposure to crystalline material does not necessarily correlate with a covalent bond being there as well. By using heating and sputtering, a stronger understanding of the surface chemistry, if any, happening between the silane and MOF can be established. Fig. 4.1A represents a theoretical scenario where the silicon atom forms a bond with three coordinate oxygens within the zirconium oxygen cluster. If a strong covalent bond is established during exposure, heating should have no impact on the capping molecule and its distinct corresponding photoelectron features. Another possibility is that the fluorinated silane molecule lingers on the MOF, but is not directly attached to anything. As seen in Fig. 3.1C, all identifying regions of the capping molecule including F 1s, Si 2p, and C 1s remain in relatively consistent intensities. Also, Zr 3d and O 1s remain minimized because the MOF surface

is no longer fully exposed to the analyzing X-rays as they were in Fig. 3.1A. At the point of analysis following heating for 15 min at 200 °C , the data fits the model seen in Fig. 4.1A. Although there was evidence of a covalent bond occurring between UiO–66 and the silane, it is unclear where that is occurring, be the surface, internal pores, or elsewhere on or within the framework. Fig. 4.1B displays a model depicting the potential impact of argon-ion sputtering in the case where there is an interfacial bond between the silane and UiO–66 MOF crystals. In summary, wherever the argon ions are positioned to bombard the sample, all chemical species on the surface monolayers will be removed. If the fluorinated silane is bound to the surface, the capping molecule's signals should drastically reduce, ideally fully diminish. This is in fact the case as seen in Fig. 3.1D. In theory, as a result of carbon, fluorine, and silicon being sputtered off the surface, the relative intensity of Zr 3d and O 1s regions should increase and look something like the nascent sample again in Fig. 3.1A. The C 1s region especially should decrease, assuming most of the adventitious chemical species is sputtered off. A potential solution to this could be rearranging the order in which the XPS multiplex is scanned in post sputtering ton ensure the sample is not collecting residual carbon. Overall, the XPS data supports our claim that there is a surface level bond between silicon and the meta organic framework. We hypothesize that this bonding interaction is occurring at the inorganic oxygens within the zirconium oxo cluster, however there is not enough information to support this claim currently. Another possibility is that this bonding is happening between the capping molecule and water molecules coordinated through linker defects on the structure. Extensive research shows UiO–66 crystals have structural defects, especially in relation to missing linkers, resulting from its complex connectivity as revealed in Figure 1.1.[2,18–19]

CHAPTER 5

CONCLUSIONS AND FUTURE WORK

We developed a surface attachment strategy for the UiO–66 MOF surface using a fluorinated silane capping molecule to form monolayers. This knowledge furthers our research for the future capping and trapping of guest molecules amongst the UiO family of metal organic frameworks. The ability to gain a controlled, on command release of guest molecules is critical for applications including therapeutic drug delivery. By tracking distinct chemical signals of the capping group using X-ray photoelectron spectroscopy, we were able to support our hypothesis that an interfacial, strong covalent bond forms between silanes and this specific MOF surface. In elucidating the surface sites of zirconium-based UiO–66, we expanded our knowledge of terminating atomic surface species and their reactivity.

In addition to information regarding UiO–66 surface chemistry, many more studies are required to get this research to its desired application, in this case being effective drug delivery methods. To begin, the experiments within this study could be further optimized to increase efficiency as it is soon to be used as a basis for future research. Of course, one should be careful regarding the XPS and its internal pressure, however three days is likely too long spent

degassing MOF samples prior to scanning. A set of control experiments could be run by evaluating various times under vacuum and in the XPS load lock and seeing how those times impact the pressure of the XPS internal chamber. Another experiment that could be done is exploring small guests to be used for proof of concept studies. Although the pores of UiO–66 are relatively small for loading and trapping guests, it could be worth seeing if something like crystal violet adsorbs using UV-Vis spectroscopy. If not, similar studies could be done using other members of the UiO family which only differ in linker composition and pore size as a result. Despite this surface science currently being limited to UiO MOFs, there are so many MOFs out there, it would be great to expand this concept to other highly stable and simple to synthesize structures. Some examples include MIL–53(Sc), MIL–53(Fe), and Bio–MOF–1. Another study that could be interesting for future researchers is comparing various silanes to determine which best blocks the pores to prevent guests from leaching. Finally, the exploration of caps that are already known to be photosensitive would be interesting to see considering it moves in the opposite direction as this project. Overall, there are many opportunities and directions to expand this work.

A

SUPPORTING INFORMATION

A.1 Introduction to the Supporting Information

To those taking over this project after my graduation, the following information is a very casual version of saying all the things that did and didn't work for me over the past year and how you can avoid doing the same and work efficiently/get results. All of this is important so please read it despite it not being fancy technical writing.

A.2 Optimizing the variables of UiO–66 synthesis

This synthesis was intended to be easy, but ended up being quite the opposite. Below I discuss in brief the variables I experimented with and what the things that may not be worth one's time to re-explore in attempts to improve the synthesis of single-crystal UiO–66.

But first, Fig. A.1 shows some pictures of the crystals as taken on the low-magnification stereoscope! As shown on the right, sometimes I got these flaky type things and I still don't really know what they are. Highly recommend putting in the pXRD (if it is functioning) if you happen to get them.

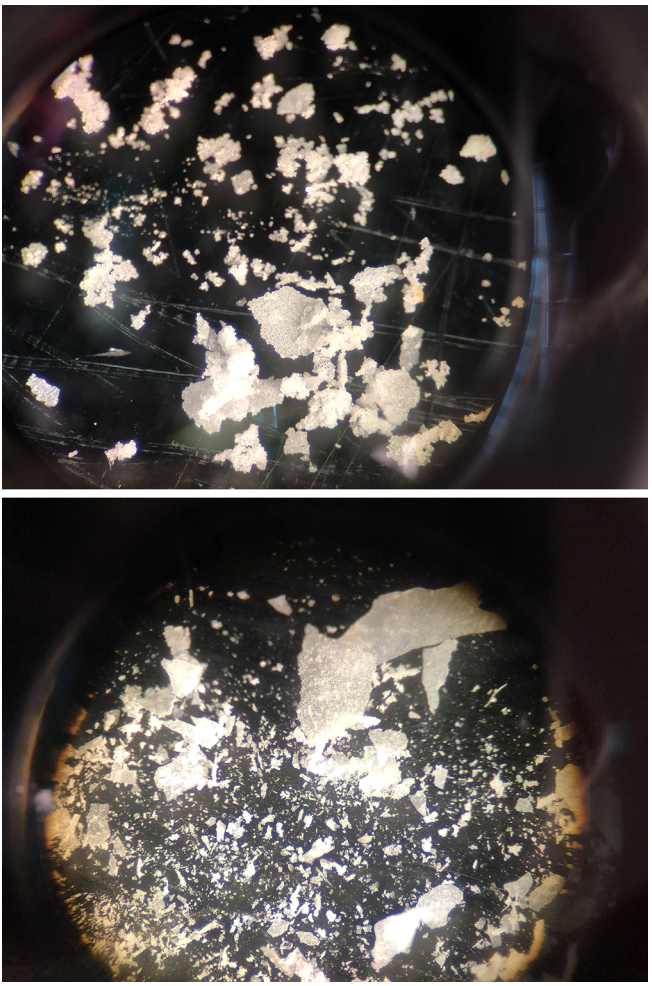

Figure A.1 Images of UiO–66 crystals from two different growth batches.

A.2.1 Reaction Vessels

1. 30 mL pressure vials with o-rings
   - regardless of the o-ring I used it burst and all solvent evaporated out
   - some of the o-rings worked sometimes but it was never consistent
2. Microwave vials
   - difficult to pump in and out of glove box
   - also many times the tops blew off during cooking because of built up pressure
3. Tube sealed glass ampoules
   - worked once or twice however they blew up other times, unreliable and hard to clean up
4. Scintillation vials
   - these ended up working the best despite there being a lack of seal in the caps (use the black ones!, didn't have as much luck with the green ones) but I compensated for that by doubling the volumes all around after tracking roughly how much volume the vials lost while cooking by marking the liquid line prior to cooking
   - be sure to dig out the inner liner of the lid, it melts and can be even harder to get the lids off

A.2.2 Oven Settings/Temperature

So the oven used to synthesize these MOFs can be a bit funky. Generally the actual internal temperature tends to be about 20–30 degrees off (that's what we found with MOF–5) but for this synthesis it was 38 °C off. I noticed that the higher it goes the more off it gets so the best way around this is gaining a comfort level for the oven and where its temperature lies using the LabVIEW temperature profiling program to monitor the temperature over time. I found that for UiO–66 synthesis setting it at 173 °C makes it stay pretty consistently internally around 135 °C. The oven can take a while to heat up so I highly recommend setting it before setting up the synthesis!! Also when you go to put the sample in to cook, the temperature drops so wait until it gets back to the set temperature to start the 48 h timer.

A.2.3 Varying Solute Concentrations

For a while I experimented around with increasing the amount of BDC and $ZrOCl_2$ with percent increases anywhere between 15 and 50% while keeping the solvent the same. I did this to hopefully get better crystals but I

don't believe this is necessary anymore because this was when other reaction conditions weren't figured out yet.

A.2.4 Solvents

Using new and more pure formic acid made such a difference in actually getting crystals. Be sure to use at least 98%.

For DEF, I didn't use to run it through a silica column prior to use but it minimizes the water in the reaction and water can impact the crystallization kinetics, size and all that.

We have been able to recover DEF from used MOF–5 runs and vacuum distill it so we can save money. However, I tried separating my DEF/formic acid/ trace DCM before and wasn't incredibly successful. Definitely worth a shot because of how expensive the solvent is. Don't just dump the DEF save it in case we eventually figure it out.

A.3 Characterization Prep/Data

A.3.1 Removing the cap lids following synthesis

This is your warning that these are so hard to open. I found that what works best is to have one hand ungloved holding the vial and the other holding the pliers and try your best to turn the vial and pliers in opposite directions. Do this in the hood because DEF is somewhat smelly. Also this usually doesn't happen by the cap just spinning off, it usually breaks and you take the cap off in pieces. However, the pressure build up can be a lot sometimes and it makes a big popping sound, so be prepared for that.

A.3.2 pXRD Mounting

Figure A.2 shows how VWR-type masking tape can be used to lower the height of a flat PFTE pXRD mounting plate to collect data from small quantities of single crystals. The tape is so the z height doesn't get thrown off too much.

A.3.3 TGA/PXRD Data

Figures A.3 and A.4 respectively present raw pXRD and TGA data for synthesized UiO–66 crystals.

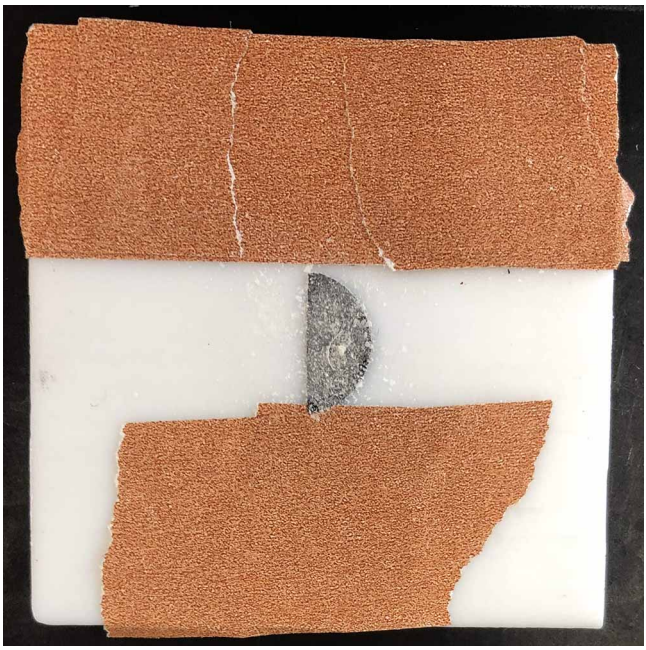

Figure A.2 VWR-type masking tape can be used to lower the height of a flat PFTE pXRD mounting plate to collect data from small quantities of single crystals.

A.4 Capping Methods

A.4.1 A failed trial on my part for maybe many reasons

I did one trial with capping where I prepared a 1 mM solution of the fluorinated silane using the 2012 bottle in the fridge and exposure time was five minutes. When we scanned it in the XPS, it very obviously had multilayers the counts were so high and sure enough when the ratios were analyzed, they were incredibly unrealistic. This sample also wasn't rinsed afterwards and wasn't put on the line to degas until the next day so that could have contributed to it as well. Basically, as soon as you're done capping, get as much liquid off as possible, rinse with DCM then get it to start drying.

A.4.2 Replication with another silane

I did try the regular procedure with a 1 mM solution of 1H,1H,2H,2H-perfluorooctyl triethoxysilane with a 30 s and 2 min and when we scanned it no fluorine showed up. Worth a shot to try again though!

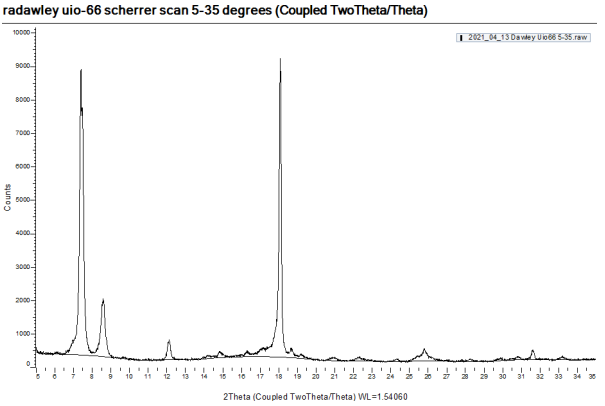

Figure A.3 pXRD trace of UiO–66 with a 0.01° step size (resolution) and a 20 s integration time at each step. This resolution and integration time is sufficiently high for a Scherrer analysis to determine grain sizes from peak widths, but may be overkill for simply verifying the presence of UiO–66 itself.

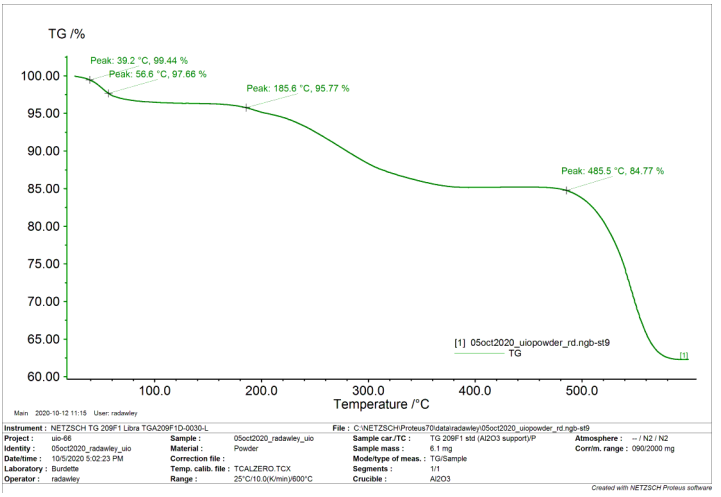

Figure A.4 TGA scan for ~6 mg of UiO-66 acquired at a heating rate of 10 °C min^{-1}.

A.4.3 Time Dependence

Once I had the procedure figured out I did a trial to see if exposure to the silane solution for 30 s, 2 min, or 5 min mattered. There wasn't a significant difference and the 5 min data was used for the data in this paper.

B

REFERENCES

1. Furukawa, H.; Cordova, K. E.; O'Keeffe, M.; Yaghi, O. M., The Chemistry and Applications of Metal-Organic Frameworks. *Science* **2013**, *341*, 1230444.
2. Marreiros, J.; Caratelli, C.; Hajek, J.; Krajnc, A.; Fleury, G.; Bueken, B.; De Vos, D. E.; Mali, G.; Maarten Roeffaers, M. B. J.; Van Speybroeck, V.; Ameloot, R.. Active Role of Methanol in Post-Synthetic Linker Exchange in the Metal-Organic Framework UiO–66. *Chem. Mater.* **2019**, *31*, 1359–1369.
3. Li, S.; Huo, F., Metal–Organic Framework Composites: From Fundamentals to Applications. *Nanoscale* **2015**, *7*, 7482–7501.
4. Yan, J.; Carl, A. D.; Maag, A. R.; MacDonald, J. C.; Müller, P.; Grimm, R. L.; Burdette, S. C., Detection of Adsorbates on Emissive MOF Surfaces with X-ray Photoelectron Spectroscopy. *Dalton Trans.* **2019**, *48*, 4520–4529.
5. Yan, J.; Homan, R. A.; Boucher, C.; Basa, P. N.; Fossum, K. J.; Grimm, R. L.; MacDonald, J. C.; Burdette, S. C., On-Demand Guest Release from MOF–5 Sealed with Nitrophenylacetic Acid Photocapping Groups. *Photochem. Photobio. Sci.* **2019**, *18*, 2849–2853.

6. Yang, J.; Wang, H.; Liu, J.; Ding, M.; Xie, X.; Yang, X.; Peng, Y.; Zhou, S.; Ouyang, R.; Miao, Y., Recent Advances in Nanosized Metal Organic Frameworks for Drug Delivery and Tumor Therapy. *RSC Adv.* **2021**, *11*, 3241-3263.

7. Alkordi, M. H.; Belmabkhout, Y.; Cairns, A.; Eddaoudi, M., Metal-Organic Frameworks for H_2 and CH_4 Storage: Insights on the Pore Geometry-Sorption Energetics Relationship. *IUCrJ* **2017**, *4*, 131-135.

8. Valenzano, L.; Civalleri, B.; Chavan, S.; Bordiga, S.; Nilsen, M. H.; Jakobsen, S.; Lillerud, K. P.; Lamberti, C., Disclosing the Complex Structure of UiO–66 Metal Organic Framework: A Synergic Combination of Experiment and Theory. *Chem. Mater.* **2011**, *23*, 1700–1718.

9. Hinterholzinger, F. M.; Wuttke, S.; Roy, P.; Preuße, T.; Schaate, A.; Behrens, P.; Godt, A.; Bein, T., Highly Oriented Surface-Growth and Covalent Dye Labeling of Mesoporous Metal-Organic Frameworks. *Dalton Trans.* **2012**, *41*, 3899–3901.

10. Zhou, Z.; Vázquez-González, M.; Willner, I., Stimuli-Responsive Metal-Organic Framework Nanoparticles for Controlled Drug Delivery and Medical Applications. *Chem. Soc. Rev.* **2021**, *50*, 4541–4563.

11. Chamundeeswari, M.; Jeslin, J.; Verma, M. L., Nanocarriers for Drug Delivery Applications. *Environ. Chem. Lett.* **2019**, *17*, 849–865.

12. Grimm, R. L.; Burdette, S. C.; MacDonald, J. C.; Scarlata, S. F., Capping Metal Organic Frameworks for Controlled, on Demand Release of Therapeutic Drugs. NIH R21 Application. Worcester Polytechnic Institute. **2019**.

13. Homan, R. A.; Hendricks, D. S.; Rayder, T. M.; Thein, U. S.; Fossum, K. J.; Claudio Vázquez, A. P.; Yan, J.; Grimm, R. L.; Burdette, S. C.; MacDonald, J. C., A Strategy for Trapping Molecular Guests in MOF–5 Utilizing Surface-Capping Groups. *Crystal Growth Des.* **2019**, *19*, 6331–6338.

14. Abánades Lázaro, I.; Haddad, S.; Sacca, S.; Orellana-Tavra, C.; Fairen-Jimenez, D.; Forgan, R. S., Selective Surface Pegylation of UiO–66 Nanoparticles for Enhanced Stability, Cell Uptake, and pH-Responsive Drug Delivery. *Chem* **2017**, *2*, 561-578.

15. Luo, Z.; Jiang, L.; Yang, S.; Li, Z.; Soh, W. M. W.; Zheng, L.; Loh, X. J.; Wu, Y.-L., Light-Induced Redox-Responsive Smart Drug Delivery System by Using Selenium-Containing Polymer@Mof Shell/Core Nanocomposite. *Adv. Healthcare Mater.* **2019**, *8*, 1900406.

16. Boissonnault, J. A.; Wong-Foy, A. G.; Matzger, A. J., Core-Shell Structures Arise Naturally During Ligand Exchange in Metal-Organic Frameworks. *J. Am. Chem. Soc.* **2017**, *139*, 14841–14844.

17. Fluch, U.; Paneta, V.; Primetzhofer, D.; Ott, S., Uniform Distribution of Post-Synthetic Linker Exchange in Metal-Organic Frameworks Revealed by Rutherford Backscattering Spectrometry. *Chem. Commun.* **2017**, *53*, 6516–6519.

18. Øien, S.; Wragg, D.; Reinsch, H.; Svelle, S.; Bordiga, S.; Lamberti, C.; Lillerud, K. P., Detailed Structure Analysis of Atomic Positions and Defects in Zirconium Metal-Organic Frameworks. *Crystal Growth Des.* **2014**, *14*, 5370–5372.

19. Trickett, C. A.; Gagnon, K. J.; Lee, S.; Gándara, F.; Bürgi, H.-B.; Yaghi, O. M., Definitive Molecular Level Characterization of Defects in UiO–66 Crystals. *Angew. Chem. Int. Ed.* **2015**, *54*, 11162–11167.

20. Schaate, A.; Roy, P.; Godt, A.; Lippke, J.; Waltz, F.; Wiebcke, M.; Behrens, P., Modulated Synthesis of Zr-Based Metal-Organic Frameworks: From Nano to Single Crystals. *Chem. Eur. J.* **2011**, *17*, 6643–6651.

21. Venable, F. P., The Chemical Behavior of Zirconium. *J. Elisha Mitchell Sci. Soc.* **1920**, *36*, 115–122.

22. Ulman, A., Formation and Structure of Self-Assembled Monolayers. *Chem. Rev.* **1996**, *96*, 1533–1554.

23. Carl, A. D.; Grimm, R. L., Covalent Attachment and Characterization of Perylene Monolayers on Si(111) and TiO_2 for Electron-Selective Carrier Transport. *Langmuir* **2019**, *35*, 9352–9363.

24. Carl, A. D.; Kalan, R. E.; Obayemi, J. D.; Zebaze Kana, M. G.; Soboyejo, W. O.; Grimm, R. L., Synthesis and Characterization of Alkylamine-Functionalized Si(111) for Perovskite Adhesion with Minimal Interfacial Oxidation or Electronic Defects. *ACS Appl. Mater. Interfaces* **2017**, *9*, 34377–34388.

25. Gao, W. R.; Zielinski, K.; Drury, B. N.; Carl, A. D.; Grimm, R. L., Elucidation of Chemical Species and Reactivity at Methylammonium Lead Iodide and Cesium Tin Bromide Perovskite Surfaces Via Orthogonal Reaction Chemistry. *J. Phys. Chem. C* **2018**, *122*, 17882–17894.

26. Martin, J. L.; Stoflet, R.; Carl, A. D.; Himmelberger, K. M.; Granados-Fócil, S.; Grimm, R. L., Quantification of Surface Reactivity and Step-Selective Etching Chemistry on Single-Crystal BiOi(001). *Langmuir* **2020**, *36*, 9343–9355.

27. Mendes, J. L.; Gao, W.; Martin, J. L.; Carl, A. D.; Deskins, N. A.; Granados-Focil, S.; Grimm, R. L., Interfacial States, Energetics, and Atmospheric Stability of Large-Grain Antifluorite Cs_2tTiBr_6. *J. Phys. Chem. C* **2020**, *124*, 24289–24297.

28. Fairley, N. Peak Fitting in XPS. `http://www.casaxps.com/help_manual/manual_updates/peak_fitting_in_xps.pdf`

29. Moulder, J. F.; Stickle, W. F.; Sobol, P. E.; Bomben, K. D., Handbook of X-ray Photoelectron Spectroscopy; Perkin-Elmer Corporation: Physical Electronics Division, 1992.

30. Jansson, C.; Hansen, H. S.; Yubero, F.; Tougaard, S., Accuracy of the Tougaard Method for Quantitative Surface Analysis. Comparison of the Universal and Reels Inelastic Cross Sections. *J. Electron Spectrosc. Relat. Phenom.* **1992**, *60*, 301–319.

31. Shirley, D. A., High-Resolution X-ray Photoemission Spectrum of the Valence Bands of Gold. *Phys. Rev. B* **1972**, *5*, 4709–4714.

32. Tougaard, S., Formalism for Quantitative Surface Analysis by Electron Spectroscopy. *J. Vac. Sci. Technol., A* **1990**, *8*, 2197–2203.

33. Negrov, D. A.; Eremin, E. N., Structuring Peculiarities of Polytetrafluoroethylene Modified with Boron Nitride When Activated with Ultrasonic Exposure. *Procedia Eng.* **2016**, *152*, 570–575.

34. Ledesma, R.; Palmieri, F.; Campbell, B.; Yost, W.; Fitz-Gerald, J.; Dillingham, G.; Connell, J., Correlation of Trace Silicone Contamination Analyses on Epoxy Composites Using X-ray Photoelectron Spectroscopy (XPS) and Laser-Induced Breakdown Spectroscopy (LIBS). *Appl. Spectrosc.* **2018**, *73*, 229–235.

35. Griffin, S. L.; Briuglia, M. L.; ter Horst, J. H.; Forgan, R. S., Assessing Crystallisation Kinetics of Zr Metal-Organic Frameworks through Turbidity Measurements to Inform Rapid Microwave-Assisted Synthesis. *Chem. Eur. J.* **2020**, *26*, 6910–6918.